Dielectric Relaxation Dynamics of High Temperature Piezoelectric Polyimide Co-polymers

A. Maceiras[1], C.M. Costa[2], A.C. Lopes[2], M. San Sebastián[3], J.M. Laza[1], J.L.Vilas[3], J.L Gómez Ribelles[4,5], R. Sabater i Serra[4], A. Andrio Balado[6], S. Lanceros-Méndez[2,*], L.M. León[1]

[1] Dpto. Química Física, Facultad de Ciencia y Tecnología, Bº Sarriena s/n, 48940-Leioa (Spain).

[2] Centro/Departamento de Física, Universidade do Minho, 4710-057 Braga, Portugal

[3] BCMaterials, Edificio 500, Parque Científico y Tecnológico de Bizkaia, 48160-Derio (Spain).

[4] Center for Biomaterials and Tissue Engineering, Universitat Politècnica de València, 46022 València, Spain

[5] Networking Research Center on Bioengineering, Biomaterials and Nanomedicine (CIBER-BBN), Valencia, Spain

[6] Departament de Física, Universitat Jaume I, 12071 Castelló, Spain

Abstract:

Polyimide co-polymers have been prepared based on different diamines as co-monomers: a diamine without CN groups and a novel synthesized diamine with two CN groups prepared by polycondensation reaction followed by thermal cyclodehydration. Dielectric spectroscopy measurements were performed and the dielectric complex function, ac conductivity and electric modulus of the co-polymers were investigated as a function of CN group content in the frequency range from 0.1 Hz to 10^7 Hz at temperatures from 25 to 260 °C.

For all samples and temperatures above 150ºC, the dielectric constant increases with increasing temperature due to increaseing conductivity. The α-relaxation is just detected for the sample without CN groups, being this relaxation overlapped by the electrical conductivity contributions in the remaining samples. For the copolymer samples and the polymer with CN groups an important Maxwell-Wagner-Sillars contribution is detected. The mechanisms responsible for the dielectric relaxation, conduction process and electric modulus response have been discussed as a function of the CN groups content present in the samples.

Keywords: Dielectric response, conductivity, electric modulus, polyimides polymer

Corresponding author: Senentxu Lanceros-Méndez, Tel: + 351 253 604 320, Fax: +351 253 604 061

Email: lanceros@fisica.uminho.pt

1. Introduction

Smart materials based on electroactive polymers (EAPs) have experienced increasing attention due to their large technological impact. In this way, new materials have been developed with excellent properties including low-density, large electromechanical response, suitable mechanical and thermal properties, leading to materials with tailored responses for specific applications [1-3]. Many of those interesting qualities of EAPs are present in piezoelectric polymers, which show fast electromechanical response, relatively low power requirements and high forces [4]. Piezoelectricity, defined as the ability of some dielectric materials to change their polarization state when subject to mechanical stress [5-7] and, reciprocally, to undergo mechanical deformation by the application of an electric field [8]. In this way, a piezoelectric material can be used for both sensor and actuator applications.

The most common and used piezoelectric polymers family corresponds to fluorinated polymers i.e., poly(vinylidene fluoride), PVDF, and its copolymers such as poly(vinylidene fluoride and trifluoroethylene), P(VDF-TrFE) [9-11]. These are semicrystalline polymers with high piezoelectric coefficients (d_{31}=20-28 pC N^{-1}) in comparison with other piezoelectric polymers such as polyamides (Nylon-11) and polyurea-9 [12, 13].

Another polymer class with large interest for high temperature applications are piezoelectric amorphous polymers, which show the glass transition at temperatures above 80 ºC [14, 15].

The origin of the piezoelectricity in amorphous polymers is different than in semi-crystalline polymers. In amorphous polymers the polarization is not in an equilibrium state, but rather in a quasi-stable state due to the freezing of molecular dipoles. In these materials, the orientation of molecular dipoles is responsible for the piezoelectricity and the glass transition temperature defines the poling process conditions [15, 16]. Other relevant factors for the piezoelectric response on amorphous polymers are the presence of a sufficient concentration of dipoles, the ability to orient these dipoles and the stability of the locking of their orientation [14].

Polyacrylonitrile (PAN) [17], poly(vinylidene cyanide–vinyl acetate) (PVDCN/VAc) [18, 19], poly(phenyl ether nitrile) (PPEN) [20], and poly(1-bicyclobutanecarbonitrile) [21] are among the most relevant examples of these piezoelectric amorphous polymers.

Due of the high glass transition temperature (T_g= 176 ºC), thermal stability and excellent mechanical and dielectric properties, the aromatic polyimide ((β-CN)APB/ODPA) polymer is an interesting amorphous piezoelectric polymer suitable for the development of high-temperature piezoelectric and pyroelectric sensors and micro-electro-mechanical system (MEMS) devices [22, 23]. Further, aromatic polyimide shows nitrile groups with large dipole moment of 4.18 D that provide a strong interaction with the applied electric field [24].

The piezoelectric effect in (β-CN)-APB/ODPA is an order of magnitude lower than the one needed for the development of practical devices, but it exhibits the thermal stability necessary to withstand conventional MEMS processing, which is a drawback for fluoropolymers [25].

Thus, new amorphous piezoelectric polyimides have been synthesized from 4,4'-oxydiphthalic anhydride and the diamines 2,4-di(3-aminophenoxy)benzonitrile (poly2-4), 2,6-bis(3-aminophenoxy)benzonitrile (poly2-6) and 1,3-bis-2-cyano-3-(3-aminophenoxy)phenoxybenzene (poly2CN). These novel polyimides differ in the position of the dipolar groups (-CN) in the aromatic ring (poly2-4 and poly2-6) and in the number of these groups in the repetitive unit (poly2-6 and poly2CN) [26, 27].

Poly2–6 and Poly2CN show low piezoelectric coefficient, d_{33}= 0.091 and 0.168 pC N^{-1} at room temperature respectively. These values strongly depend on the number of dipole CN groups in the repetition unit, as well as on the imidization and the poling processes [28]. The dielectric and piezoelectric properties of these amorphous polyimides was addressed in [29] showing that the frozen-in polarization is mainly due to dipolar orientation of the dipolar CN groups, which in turn contribute to the piezoelectric response.

In this way and in order to improve the dielectric and piezoelectric response of these polyimides, new co-polymers were produced based on different diamines as co-monomers: a diamine without CN groups and a novel synthesized diamine with two CN groups. Thus, due to the large potential of this newly developed materials, a deep characterization and understanding of the dielectric response is essential for the development of applications. This work reports on the dielectric relaxation spectrum, electrical conductivity and electric modulus of the different co-polymers as a function of frequency and temperature.

2. Experimental:

2.1. Reagents:

The commercial products used for the synthesis of monomers and polymers were 4,4'-oxydiphthalic anhydride (ODPA), 2,6-dichlorobenzonitrile, resorcinol, potassium carbonate, dimethylsulfoxide (DMSO), dimethylacetamide (DMAc), 2,6-dichlorobenzonitrile, 3-aminophenol (supplied by Aldrich), and 1,3-Bis(3-aminophenoxy)benzene (Tokyo Chemical Industry, TCI). All the products were used as received except potassium carbonate, which was dried at 100 ºC before use.

2.2. Synthesis:

The synthesis of the polyimides was carried out by starting the reaction between the dianhydride and two diamines, the 1,3-bis-2-cyano-3-(3-aminophenoxy) phenoxybenzene (diamine 2CN) [26] and the 1,3-Bis(3-aminophenoxy)benzene (diamine 0CN). Figure 1 shows the structure of both diamines.

Polyimides were synthesized using both single diamines (0CN diamine and diamine 2CN) and co-polyimides by using the diamines in different proportions. A two-step procedure was used. In the first step, a nucleophilic attack of amine groups toward carbonyl groups in the dianhydride produces the co-poly(amic acid); in the second step, the cyclodehydration reaction caused by thermal treatment gives rise to the co-polyimide. The general scheme of the synthesis of a co-polyimide is shown in Figure 2.

After synthesis, the corresponding polyimides were obtained by thermal imidization of the poly(amic acid) and co-poly(amic acid).

With a silicon designed mold with a centered cavity of dimensions 45x45 mm, poly(amic acid)'s imidization and film fabrication was carried out simultaneously. Thus, 0.6 g of poly(amic acid) or co-poly(amic acid) was dissolved into 6 cm^3 N,N-dimethylacetamide (DMAc). Later, the poly(amic acid) was cast to form ~150 µm films that were subsequently thermally imidizated, according with the thermal treatment represented in Figure 3. The thermal treatment was chosen for solvent evaporations at a sufficiently low rate to avoid bubble formation during the curing step.

Polymer 0CN, co-polymer 0CN/2CN (60/40) and 0CN/2CN (50/50) and polymer 2CN were prepared and will be called hereafter 0CN, 0CN/2CN (60/40), 0CN/2CN (50/50) and 2CN, respectively. The results of the both co-polymers are very similar and for this reason only will be shown the figures for co-polymer 0CN/2CN (50/50).

2.3. Characterization:

Dielectric spectroscopy measurements were carried out using an impedance analyzer Alpha-S trough the measurement of the capacitance (C) and the loss factor (tan δ). The temperature control was performed by a Quatro Cryosystem from Novocontrol GmbH. Circular conducting gold electrodes (10 mm diameter) were deposited onto both sides of each sample, to form a parallel plate capacitor. The electrodes were deposited by magnetron sputtering with a Polaron Coater SC502 under an Argon atmosphere. The sample cell with active head dielectric converter was mounted on a cryostat (BDS 1100) and exposed to a heated gas stream evaporated from a liquid nitrogen Deward. The isothermal experiments were performed from 25°C to 260 °C (thermal stability: 0.5 °C) in 5 °C steps. The complex dielectric permittivity $\varepsilon^* = \varepsilon' - i\varepsilon''$ was determined as a function of frequency (10^{-1}–10^7 Hz) through the following equations:

$$\varepsilon' = \frac{Cd}{\varepsilon_0 A} \tag{1}$$

and

$$\varepsilon'' = \tan\delta * \varepsilon' \tag{2}$$

where C is the capacitance, ε’ is real part of the dielectric constant, ε’’ is imaginary part of the dielectric constant, ε_0 is the permittivity of the free space (8.85×10^{-12} F m^{-1}), and d and A are the sample thickness and electrode area, respectively.

3. Results and discussion

3.1. Overall dielectric response

The dielectric response will be discussed highlighting first the temperature dependent features and then the frequency dependence ones.

3.1.1. Temperature dependence

Figure 4 shows the evolution of real (ε′) and imaginary parts (ε″) of the dielectric function as a function of temperature at different frequencies for the different samples. For all samples, the real part of the dielectric constant increases as frequency decreases for all temperature range due to the increasing inability of the dipoles to orient with the rapidly varying applied electric field as frequency increases [30]. The same trend is found for the dc conductivity contribution to the imaginary part of the dielectric permitivitty, the peak due to dipolar relaxation appearing in ε″ shifting to higher temperatures with increasing frequency.

The dielectric response is practically constant up to 150 ºC for all samples, independently of the frequency (Figure 4). No significant differences are observed between the dielectric response of the 0CN/2CN (60/40) and 0CN/2CN (50/50) co-polymer so just the data for the 50/50 co-polymer will be shown.

The dielectric constant for 0CN/2CN (50/50) co-polymer shows a low frequency peak (up to ~100 Hz) around 175 ºC as is observed in figure 4c). The reason of this peak in both co-polymers is due to a decrease of the ionic mobility related to imidization of the dianhydride groups [28]. This decrease cannot be attributed to a relaxation process, as it is characterized by a peak in the real part of the dielectric constant.

The room temperature values of the dielectric response are summarized in table 1 for a frequency of 1 kHz, together with the values at 200 ºC. The room temperature values are in agreement with the values found in the literature for the polyimides [31]. The differences observed of the dielectric constant for the 0CN and 2CN polymers at room temperature are fully attributed to the presence of the nitrile groups in the 2CN polymer.

For temperatures above 150 ºC and for all samples, the dielectric constant increases with increasing temperature due to enhancement of the dipolar mobility and increased conductivity, i.e. dielectric losses (Figure 4 b), d) and f)), as reflected in the comparison of the values of the dielectric response at room temperature and 200 ºC presented in table 1.

The insert of Figure 4b) for the 0CN polymer shows the α-relaxation above 150 ºC related to the glass transition and attributed to the cooperative segmental motions of the amorphous sample [32].

The dynamics of the α-relaxation observed in the 0CN polymer (Figure 4b) was analyzed in the scope of the Vogel-Fulcher-Tammann (VTFH) formalism [33]:

$$\tau(T) = \tau_0 e^{\frac{E_{VFTH}}{k_B(T-T_0)}} \quad (3)$$

where τ is the relaxation time, E_{VFTH} is the VFTH energy, k_B the Boltzmann constant and T_0 is the critical temperature at which molecular motions become infinitely slow [34].
From the VTFH fitting parameters, the fragility parameter [35] can be calculated:

$$m = \frac{E_{VTFH} / kT_g}{(\ln 10)\left(1 - T_0 / T_g\right)^2} \quad (4)$$

where *m* is an indication of the steepness of the variation of the material properties (viscosity, relaxation time, …) as T_g is reached. A high *m* value defines a fragile material whereas a strong material is characterized by small *m* values [36].
The $m(T_g)$ value was determined at the glass transition temperature (T_g) where the relaxation time is equal to 100 s.
The α-relaxation observed for the 0CN polymer was thus obtained from the fitting with equation 3 shown in Figure5. The obtained fitting parameters are shown Table 2.

The results shown in Table 2 indicate that the cooperative motions of the amorphous chains (τ_0 value) are very slow and with high VFTH energy. The glass transition temperature determined through this formulation is very similar the value determined by DSC technique (T_g=176 ºC) [27]. The fragility parameter for the 0CN polymer is equal to the one observed for the semi crystalline polymer α-PVDF [37]. T_0 is typically defined as the real glass transition temperature, which is found to be 30-70 ºC below the measured T_g. For 0CN polymer, T_0 is below T_g and the difference of both temperatures is 56 ºC[32]. For 2CN polymer and the respective co-polymers, the α-relaxation is not detected due to the overlapping of the electric conductivity contributions, particularly high at high temperatures and low frequencies.

3.1.2. Frequency dependence

In the frequency domain representation (Figure 6), ε'' versus frequency at isothermal conditions is used for the identification of the dipolar relaxations. Amorphous polymers show different motional processes visible the ε'' versus ν representation as peaks (Figure 6).

Figure 6 show the imaginary part of the dielectric function for the different samples. For the 0CN polymer (Figure 6a) the α-relaxation is clearly identified. A detailed representation of this relaxation is represented in Figure 6b (above 195 ºC), where it is observed that the α-relaxation is shifted to higher frequencies as temperature increases. This relaxation is related to a long timescale and corresponds to an overall structure rearrangement of the system [38].

For the 0CN polymer (Figure 6a) and for low frequencies and temperatures below 195 ºC, the conductivity contribution in the frequency domain is prominent, being this contribution the main one for the rest of the samples (Figure 6c-d). The α-relaxation is not resolved in the copolymers and the 2CN polymer due to the overlapping of dielectric relaxation and conductivity contributions. The conductivity contribution decreases with decreasing temperature, being larger for low frequencies. Further, it can be stated an increase of the conductivity associated to the addition of the nitrile (-CN) dipolar group. As it will also be shown later, the conductivity effect contributing to the increase of the dielectric loss in all samples (Figure 6) is also influenced by the Maxwell-Wagner-Sillars process, i.e., the charges blocked at internal phase boundaries, related to the different constitutes of the co-polymers, submicropores or at the interface between the sample and the electrodes (electrode or space charge polarization) [39].

3.2. Overall conductivity

In order to further explain relaxation dynamics of charge carriers and the characteristics of the ionic conduction with certain influence of a MWS process, it is more appropriate the representation of frequency and temperature dependence of complex conductivity, σ*, which can be calculated from the dielectric function through the following equation:

$$\sigma^* = i\varepsilon_0\omega\varepsilon^*(\omega) = i\varepsilon_0\omega\left(\varepsilon'(\omega) - \varepsilon''(\omega)\right) = \varepsilon_0\omega\varepsilon''(\omega) + i\varepsilon_0\omega\varepsilon'(\omega) \quad (6)$$

Thus, the real part of the conductivity is given by:

$$\sigma'(\omega) = \varepsilon_0 \omega \varepsilon''(\omega) \quad (7)$$

and the imaginary part of the conductivity is given by:

$$\sigma''(\omega) = \varepsilon_0 \omega \varepsilon'(\omega) \quad (8)$$

where ε_0 (8.85×10^{-12} Fm^{-1}) is the permittivity of free space and $\omega = 2\pi f$ is the angular frequency.

The real and imaginary parts on the complex electrical conductivity, σ*(ω), is plotted in Figure 7 as a function of frequency for several temperatures.

For all samples it is observed two well identified regimes that depend of the temperature and frequency (Figure 7). For low temperatures up to T=135 ºC, the conductivity increases rapidly with increasing frequency. For temperatures above T=185 ºC, it is observed a plateau, in which the conductivity (Figure 7a), c), e) and g)) is nearly independent of frequency in the low frequency region, being this regime thus dominated by the dc conductivity.

At higher frequencies and temperatures a power law dependence of the ac electrical conductivity is observed, which is related to hopping transport of localized charge carriers [40]. The electrical conductivity is larger for the samples with larger CN content. There are also found deviations from a pure plateau region in the low frequency conductivity spectrum (Figure 7) that can be attributed to electrode polarization effects and to the charge blocking at the interphase regions as well as the imperfections (i.e. submicropores due to the solvent evaporation process) that occur due to the polymer processing method.

This behaviour can be thus ascribed to contribution of MWS and, at still higher frequencies, to dipolar relaxation modes. It is evident that 2CN polymer (Figure 7e) and the co-polymers (Figure 7c) shows higher conductivity due of the presence of the nitrile groups in the polymer chain in comparison of the 0CN polymer (Figure 7a).

The presence of the nitrile group affects also the MWS relaxation that is related to the existence and blocking of free charge carriers inside the system. The MWS relaxation becomes increasingly important at high temperatures, reflecting the enhancement of the mobility of charge carriers.

The ac conductivity at constant temperature as a function of frequency can be expressed as [41]:

$$\sigma'(\omega) = \sigma_{dc} + A\omega^n \quad (9)$$

where σ_{dc} is the DC conductivity, A is the pre-exponential factor and n is the fractional exponent ($0 < n < 1$) that depends of the temperature. The value of n is used to a better understanding of the conduction or relaxation mechanism in insulating materials [42].

Figure 8, left shows that σ_{dc} increases with increasing temperature in a similar way for all samples. This behavior reflects the mechanism of charge transport of carriers. There are not significant differences in values or behavior for the two co-polymers, the values of the conductivity being intermediate between the ones obtained for the pure polymers. With respect to the two homopolymers, 2CN polymer shows higher σ_{dc} than 0CN polymer in all temperature range, attributed to the presence of the nitrile group.

In relation to the n parameter, it decreases with increasing temperature until 227 ºC for all polyimide films. Independently of the sample type, the n parameter ranging between 0.6 and 0.9, as corresponds to a hopping conductivity process (Figure 8, right) [43].

In this way, the transport mechanism of the samples is thermally activated hopping across an energy barrier. For the evaluation of the dependence of the ac conductivity with temperature at different frequencies, the Dyre model [44] (random free energy barrier model or symmetric model) was applied [45]:

$$\sigma(T) = Be^{\frac{E_a}{k_B T}} \quad (10)$$

where B is a pre-exponential factor identified as the attempt frequency, E_a is the activation energy of the process, T is temperature and k_B is the Boltzmann constant.

The application of the Dyre model in order to obtain the dependence of the electrical conductivity on the reciprocal temperature at different frequencies is shown in Figure 9. and the activation energy, E_a, calculated are plotted in Figure 10.

Figure 9 shows the ac conductivity for the 0CN polymer (Figure 9a), with noteworthy differences from the remaining polymers in both temperature dependence behaviour (Figures 9b and 9c) and activation energy (Figure 10)

It can be observed that for the co-polymers samples and the 2CN polymer, the activation energy is larger (with the exception of the higher frequencies) and decrease with increasing of the frequencies. This fact is linked to the mobility of nitrile groups, determining the electrical response of these samples. The activation energy for 0CN shows a strong decrease for low frequencies with respect to the other samples, increasing for frequencies above 10 Hz. This variation can be ascribed the presence of free charges contributing to the MWS relaxation processes, as will be shown in the next section.

3.3. Electric modulus formalism

In order to further explore the conduction behaviour (ionic conductivity and interfacial polarization, the so-called Maxwell-Wagner-Sillars (MWS) effect), the electric modulus formalism, M^* [46], is the most appropriate representation and can be used for differentiate dielectric relaxation processes from long-range conductivity [47]. Typically, for samples with higher conductivity, one high peak related to the conductivity is detected in the frequency spectra of the imaginary electric modulus formalism, M´´ in the same temperature interval where the conductivity process is shown in the imaginary part of the dielectric function (ε'').

The electrical modulus, M^*, is defined as the reciprocal of the complex relative permittivity, $\varepsilon^*(\omega)$:

$$M^*(\omega) = 1/\varepsilon^*(\omega) = M'(\omega) + iM''(\omega) = \frac{\varepsilon'(\omega)}{\varepsilon'^2(\omega)+\varepsilon''^2(\omega)} + i\frac{\varepsilon''(\omega)}{\varepsilon'^2(\omega)+\varepsilon''^2(\omega)} \quad (11)$$

where M´, M´´ are the real and imaginary components of the complex electric modulus, respectively.

For a dipolar relaxation process, equation (10) yields a relaxation peak in M'' and a drop of M' with decreasing frequency. On the other hand for a pure dc conduction process in which ε' is independent of frequency and ε'' is inversely proportional to frequency, equation (11) yields the same frequency dependence than in a Debye single relaxation

time process. The imaginary component of dielectric modulus can be used to define a relaxation time for conductivity

$$M'' = M_{\infty} \frac{\omega \tau_{Cond}}{1 + (\omega \tau_{Cond})^2} \tag{12}$$

MWS processes also yields narrow relaxation processes in electric modulus formalism while presenting a clear increase of ε' with decreasing frequency.

Deviations with respect to the Debye single relaxation time model in the electric field relaxation due to motions of charge carriers are generally described by the empirical Kohlrausch-Williams-Watts (KWW) function [48, 49]:

$$M^*_{\beta KWW}(\omega) = M_{\infty}\left[1 - \int_0^{\infty} \exp(i\omega t)(-d\phi/dt)dt\right] \tag{13}$$

with

$$\phi(t) = \exp\left[-(t/\tau_M)^{\beta}\right], \quad 0 < \beta \leq 1, \tag{14}$$

where τ_M and β are the conductivity relaxation time and the Kohlrausch exponent, respectively. The smaller the value of β, the larger the deviation of the relaxation with respect to a Debye-type relaxation (β=1).

Values of the Kohlrausch exponential parameter β in the KWW function were approximately estimated by means of [50]:

$$\beta = 1.14/w \qquad , \tag{15}$$

where w is the peak's full width at half maximum.

The temperature dependence of the real M´ and imaginary M´´ electric modulus for various frequencies is shown in Figure 11 for all samples.

The M* spectra of the 0CN sample clearly shows the space charge mechanism at low frequencies appearing as a step in M' and a narrow peak in M'' (the value of the Kohlrausch parameter calculated for this peak using equation 14 is β=0.9) followed by the dipolar relaxation process appearing as a second step in M' and a broad peak in M'' (Figures 11a and 11b). The relaxation time for conductivity τ_{Cond} is related to the

frequency at which the peak in M'' appears, f_{max}, (equation 12) trough $\tau_{Cond}=1/2\pi f_{max}$. The temperature dependence of f_{max} has been represented in Figure 5.

In the 2CN samples, space charge and dipolar relaxation are closer to each other and partially overlaps. In addition, the low frequency M'' peak, due to free charge motions is broader than in the 0CN samples (Kohlrausch parameter calculated for this peak using equation 14 is $\beta=0.60$ at 155 ºC). The peak of this process appears at lower temperatures than in the 0CN sample and shows a smaller temperature variation indicating that lower energy barriers hinder the motions of space charge carriers in the 2CN sample. The presence of the high frequency relaxation can be noticed above 175 ºC by the loss of the symmetry of the conductivity peak by the lifting of its high frequency side. At higher temperatures the shape of the M'' plot clearly shows the overlapping of two processes. Some indications of the presence of this high frequency peak could be observed in the permittivity plot in Figure 6e. Interestingly, the drop of the real part of permittivity that takes place in the 2CN sample in the temperature interval between 225 and 250ºC that was ascribed to the imidization of dianhydride groups [28] is not reflected in the dielectric modulus formalism.

The behaviour of the copolymer is in between that of the two components. The space charge M'' peak is even broader than in 2CN sample and Kohlrausch parameter is only $\beta=0.5$. The presence of the high frequency dipolar relaxation is now clear above 200 ºC and the sharp decrease of ε' due to the imidization of dianhydride groups has not a counterpart in M'. Instead, for the co-polymers and 2CN polymer (Figure 11 b-d), two peaks appear above 205 °C, which shift to higher frequency with increasing temperature, both samples showing similar relaxation process behaviour. The peak observed for all temperatures at low frequencies represents the movement of charge carriers over a long distance, i.e., charge carriers can perform successful hopping from one site to a neighboring site [51]. For higher frequencies, the observed peak indicate the presence of charges confined to local motions [47].

Conclusions

Thin films of polyimide polymers have been produced by by polycondensation reaction followed by thermal cyclodehydration, based on different diamines as co-monomers: a diamine without CN groups and a novel synthesized diamine with two CN groups.

The dielectric properties of the samples are determined by the presence of the CN groups. The dielectric constant, ε′, increases with increasing temperature for all samples. The α-relaxation is only detected for 0CN polymer being overlapped by the large conductivity contributions in the remaining samples. The conductivity behavior reflects the mechanism of charge transport behavior. For co-polymers and 2CN polymer at high temperature, the spectrum is dominated by ionic conductivity and interfacial polarization. The differences observed for the activation energy between the samples in the conductivity process is attributed to the presence of the MWS relaxation process. The presence of the CN group in the co-polymers and 2CN polymer increases the MWS contribution as detected in the electric modulus formalism plots.

Acknowledgements

This work was supported by FEDER through the COMPETE Program and by the Portuguese Foundation for Science and Technology (FCT) in the framework of the Strategic Project PESTC/FIS/UI607/2011 and grants SFRH/BD/ 62507/2009 (A.C.L.) SFRH/BD/68499/2010 (C.M.C.). The authors also thank funding from "Matepro – Optimizing Materials and Processes", ref. NORTE-07-0124-FEDER-000037", co-funded by the "Programa Operacional Regional do Norte" (ON.2 – O Novo Norte), under the "Quadro de Referência Estratégico Nacional" (QREN), through the "Fundo Europeu de Desenvolvimento Regional" (FEDER). RSS acknowledge the support of the Spanish Ministry of Economy and Competitiveness through the project MAT2012-38359-C03-01 (including the FEDER financial support).

Authors also thank the Basque Country Government for financial support (ACTIMAT project, ETORTEK Program, IE13-380, and Ayudas para Grupos de Investigación del Sistema Universitario Vasco Program, IT718-13).

References

1. Schwartz M. Smart Materials: Taylor & Francis, 2008.
2. Addington M and Schodek D. Smart Materials and Technologies in Architecture: Taylor & Francis, 2012.

3. Leng J-S, Lan X, Lu H-B, and Liu Y-J. International Journal of Modern Physics B 2010;24(15n16):2351-2356.
4. Vives AA and Arnau A. Piezoelectric Transducers and Applications: Springer, 2008.
5. Heywang W, Lubitz K, and Wersing W. Piezoelectricity: Evolution and Future of a Technology: Springer, 2008.
6. Ikeda T. Fundamentals of Piezoelectricity: Oxford University Press, Incorporated, 1996.
7. Neugschwandtner G S, Schwödiauer R, Bauer-Gogonea S, Bauer S, Appl. Phys. A 2000, 70: 1
8. Nye JF. Physical Properties of Crystals: Their Representation by Tensors and Matrices: Clarendon Press, 1985.
9. Martins P, Lopes AC, and Lanceros-Mendez S. Progress in Polymer Science 2014;39(4):683.
10. Silva MP, Costa CM, Sencadas V, Paleo AJ, and Lanceros-Méndez S. Journal of Polymer Research 2011;18(6):1451-1457.
11. Gomes J, Nunes JS, Sencadas V, and Lanceros-Mendez S. Smart Materials and Structures 2010;19(6):065010.
12. Furukawa T. Electrical Insulation, IEEE Transactions on 1989;24(3):375-394.
13. Sessler GM. The Journal of the Acoustical Society of America 1981;70(6):1596-1608.
14. Sessler GH, Sessler GM, Broadhurst MG, and Gerhard-Multhaupt R. Electrets: Laplacian Press, 2000.
15. Ounaies Z, Young Jennifer A, and Harrison Joycelyn S. An Overview of the Piezoelectric Phenomenon in Amorphous Polymers. Field Responsive Polymers, vol. 726: American Chemical Society, 1999. pp. 88-103.
16. Chûjô R. Molecular Design of Amorphous Piezoelectric Polymers with the Aid of NMR. In: Prasad P and Nigam J, editors. Frontiers of Polymer Research: Springer US, 1991. pp. 371-376.
17. Von Berlepsch H, Kunstler W, Wedel A, Danz R, and Geiss D. Electrical Insulation, IEEE Transactions on 1989;24(2):357-362.
18. Seo I. Ferroelectrics 1995;171(1):45-55.
19. Mirau PA and Heffner SA. Polymer 1992;33(6):1156-1161.

20. Takahashi T, Kato H, Ma SP, Sasaki T, and Sakurai K. Polymer 1995;36(20):3803-3808.
21. Hall HK, Jr., Chan RH, Oku J, Hughes OR, Scheinbeim J, and Newman B. Polymer Bulletin 1987;17(2):135-136.
22. Park C, Ounaies Z, Wise KE, and Harrison JS. Polymer 2004;45(16):5417-5425.
23. Furuya Y, Su J, Takeuchi I, Varadan VK, and Ulicny J. Materials and Devices for Smart Systems II: Cambridge University Press, 2006.
24. van Krevelen DW. Properties of Polymers: Elsevier Science, 2012.
25. Simpson J, Ounaies Z, and Fay C. MRS Online Proceedings Library 1996;459.
26. Gonzalo B, Vilas JL, Breczewski T, Pérez-Jubindo MA, De La Fuente MR, Rodriguez M, and León LM. Journal of Polymer Science Part A: Polymer Chemistry 2009;47(3):722-730.
27. Sebastián MS, Gonzalo B, Breczewski T, Vilas JL, Pérez-Jubindo MA, De La Fuente MR, and León LM. Ferroelectrics 2009;389(1):114-121.
28. Gonzalo B, Breczewski T, Vilas JL, Perez-Jubindo MA, De La Fuente MR, Dios JR, and León LM. Ferroelectrics 2008;370(1):3-10.
29. Gonzalo B, Vilas JL, San Sebastián M, Breczewski T, Pérez-Jubindo MÁ, de la Fuente MR, Rodríguez M, and León LM. Journal of Applied Polymer Science 2012;125(1):67-76.
30. Sakthivel S, Shekar BC, Mangalaraj D, Narayandass SK, Venkatachalam S, and Prabhakaran PV. European Polymer Journal 1997;33(10–12):1747-1752.
31. Muruganand S, Narayandass SK, Mangalaraj D, and Vijayan TM. Polymer International 2001;50(10):1089-1094.
32. Kremer F and Sch?nhals A. Broadband Dielectric Spectroscopy: Springer, 2003.
33. Scherer GW. Relaxation in Glass and Composites: Krieger Publishing Company, 1991.
34. Boyd RH. Polymer 1985;26(3):323-347.
35. Lanceros-Mendez S, Moreira MV, Mano JF, Schmidt VH, and Bohannan G. Ferroelectrics 2002;273(1):15-20.
36. Firmino Mendes S, Costa CM, Sencadas V, Serrado Nunes J, Costa P, Gregorio R, Jr., and Lanceros-Méndez S. Applied Physics A 2009;96(4):899-908.
37. Lopes AC, Costa CM, Serra RSi, Neves IC, Ribelles JLG, and Lanceros-Méndez S. Solid State Ionics 2013;235(0):42-50.

38. Chan RK, Pathmanathan K, and Johari GP. The Journal of Physical Chemistry 1986;90(23):6358-6362.
39. Lu H and Zhang X. Journal of Macromolecular Science, Part B 2006;45(5):933-944.
40. Lunkenheimer P, Götzfried T, Fichtl R, Weber S, Rudolf T, Loidl A, Reller A, and Ebbinghaus SG. Journal of Solid State Chemistry 2006;179(12):3965-3973.
41. Jonscher AK. Nature 1977;267(5613):673-679.
42. Deligöz H, Yalcinyuva T, Özgümüs S, and Yildirim S. Journal of Applied Polymer Science 2006;100(1):810-818.
43. Nada AMA, Dawy M, and Salama AH. Materials Chemistry and Physics 2004;84(2–3):205-215.
44. Dyre JC and Schrøder TB. Reviews of Modern Physics 2000;72(3):873-892.
45. Dyre JC. Journal of Applied Physics 1988;64(5):2456-2468.
46. Tsangaris GM, Psarras GC, and Kouloumbi N. Journal of Materials Science 1998;33(8):2027-2037.
47. Molak A, Paluch M, Pawlus S, Klimontko J, Ujma Z, and Gruszka I. Journal of Physics D: Applied Physics 2005;38(9):1450.
48. Ngai KL and Martin SW. Physical Review B 1989;40(15):10550-10556.
49. Lu H, Zhang X, and Zhang H. Journal of Applied Physics 2006;100(5):054104.
50. Dixon PK. Physical Review B 1990;42(13):8179-8186.
51. Prakash T, Prasad KP, Kavitha R, Ramasamy S, and Murty BS. Journal of Applied Physics 2007;102(10).

Tables and table captions

Table 1 – Dielectric constant for the samples at 1kHz.

	T=25 ºC		T=200 ºC	
Sample	ε'	ε''	ε'	ε''
0CN	2.8	0.003	3.8	0.3
0CN/2CN (60/40)	3	0.009	8	3.5

0CN/2CN (50/50)	2.4	0.006	8	3.5
2CN	4.1	0.007	21	17

Table 2: VFTH fitting parameters of the α-relaxation of the 0CN polymer

Samples	τ_0 (s)	E_{VFT} (eV)	T_0 (K)	T_g (K)	*M*
0CN	5.1×10^{-12}	0.15	387	443	105

Figures and Figure Captions

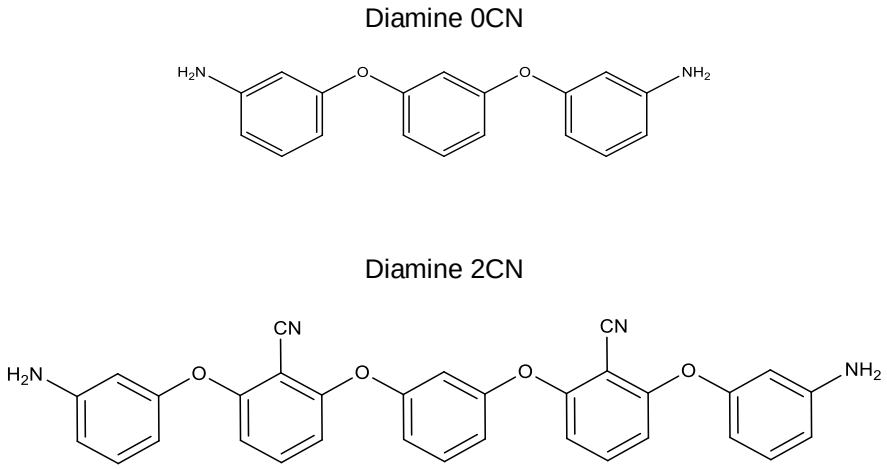

Figure 1 - Chemical structure of the used diamines.

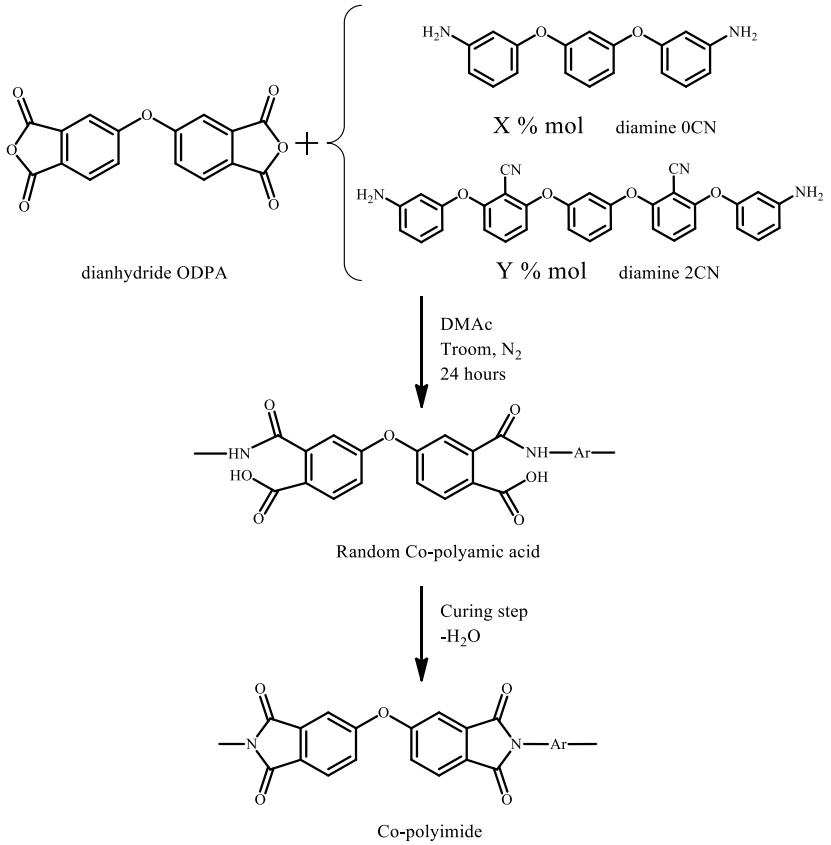

Figure 2 - Scheme of the two-step reaction used for the synthesis of the co-polyamines

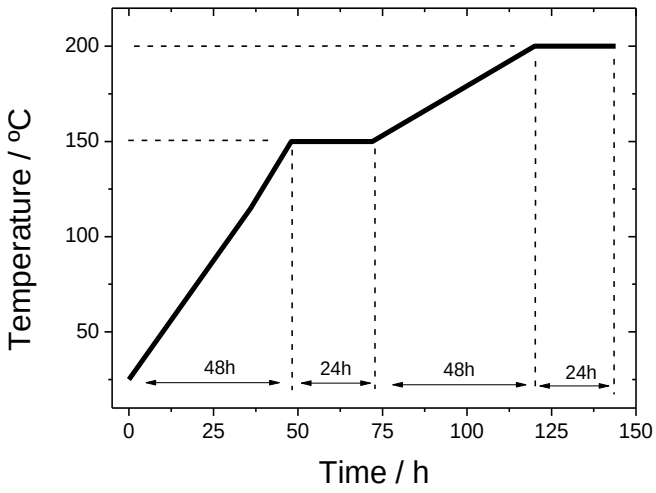

Figure 3 – Heating cycle applied for the preparation of the polyimide co-polymers

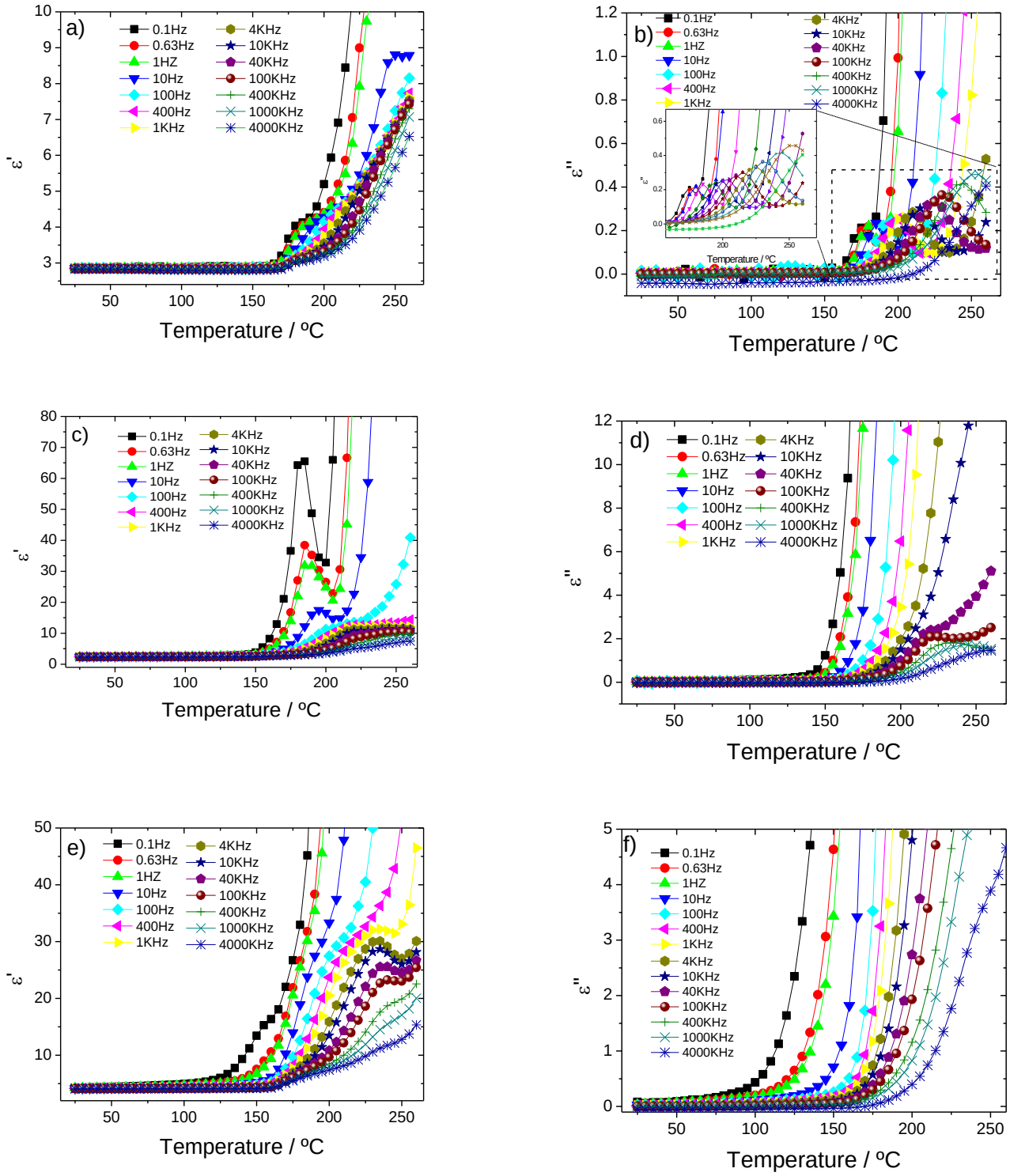

Figure 4 - Real and imaginary part of the dielectric function as a function of temperature at different frequencies, for 0CN (a-b), 0CN/2CN (50/50) (c-d) and 2CN (e-f).

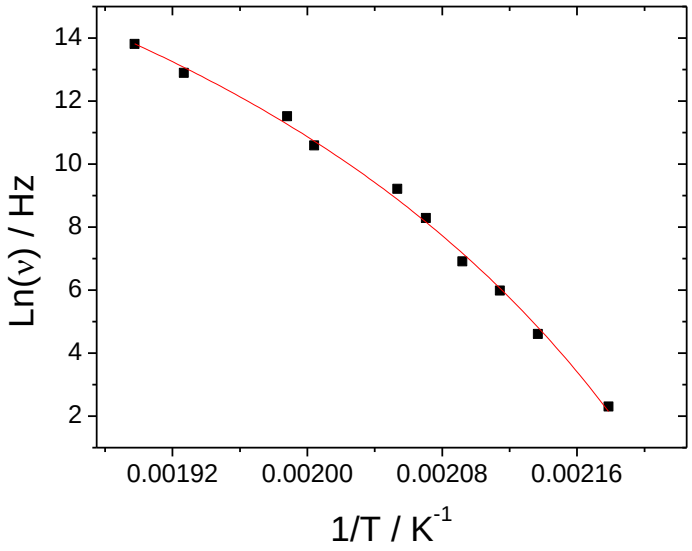

Figure 5 - VFTH fitting for the α-relaxation of 0CN polymer

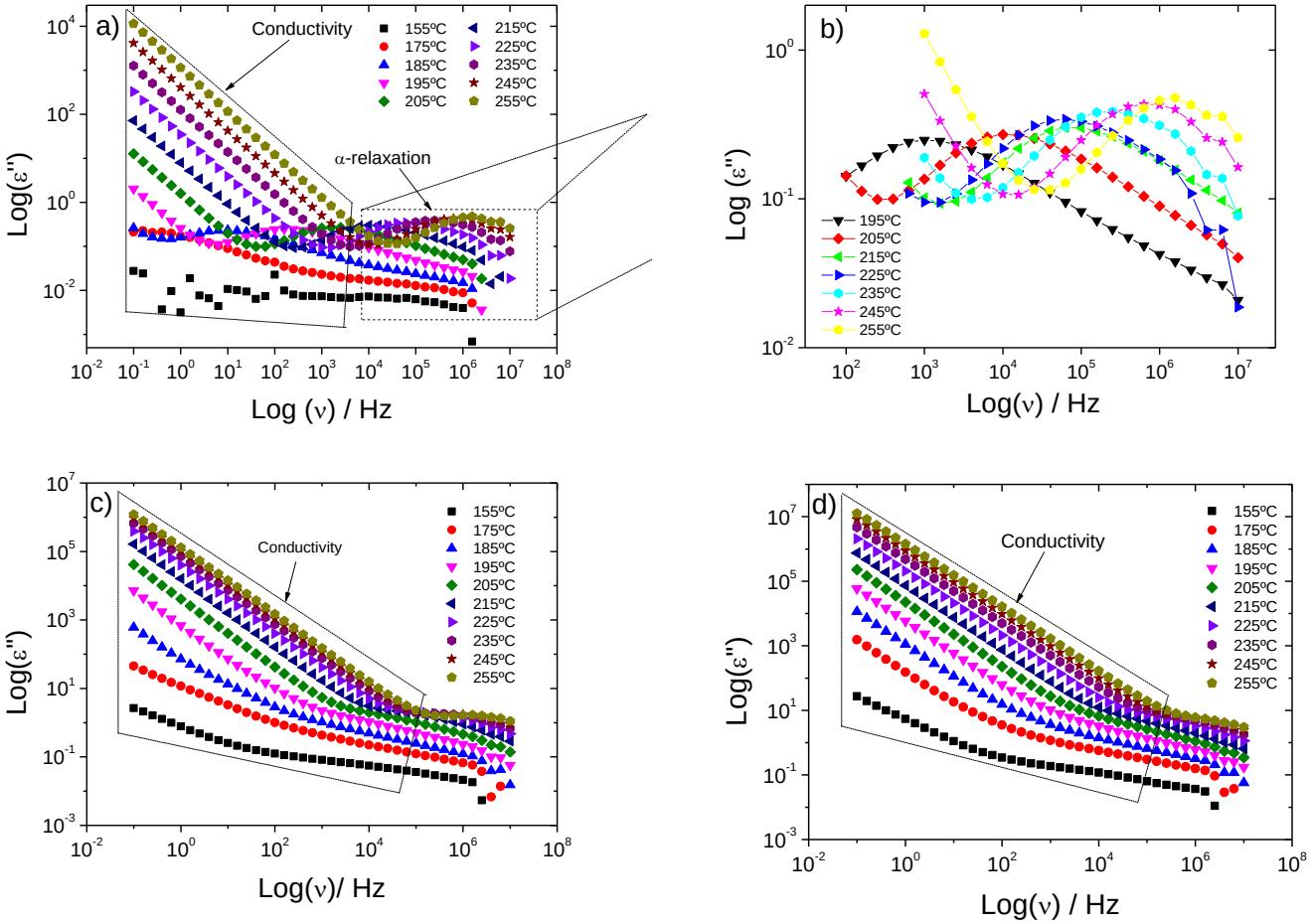

Figure 6 - Frequency dependence of the imaginary part of the dielectric function of (a) 0CN, (c), 0CN/2CN (50/50) and (d) 2CN at various temperatures. Details of the α-relaxation in 0CN are showed in (b).

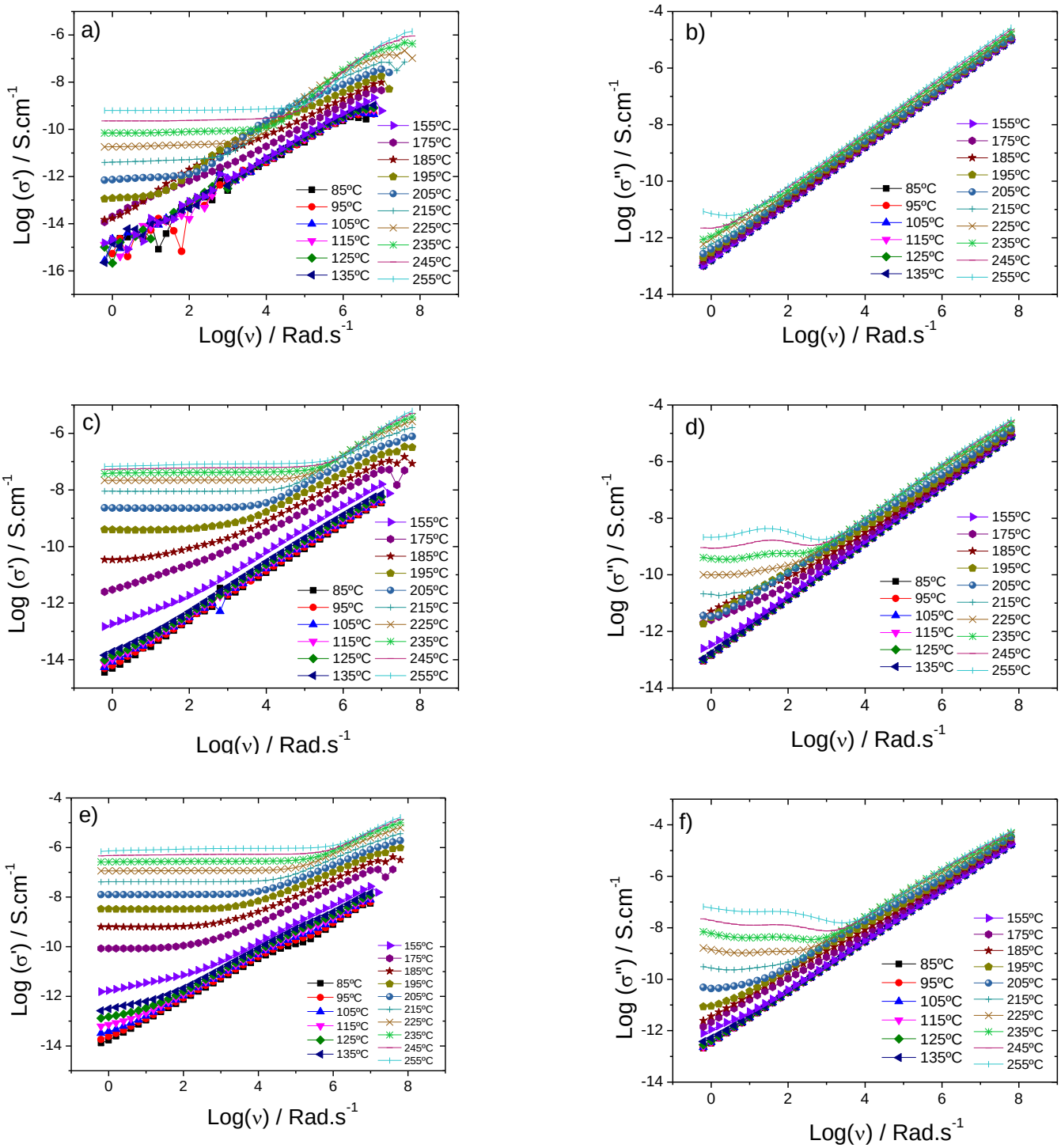

Figure 7 - Real and imaginary parts of the electrical conductivity as a function of frequency at different temperatures for 0CN (a) and (b), 0CN/2CN (50/50) (c) and (d), and 2CN (e) and (f).

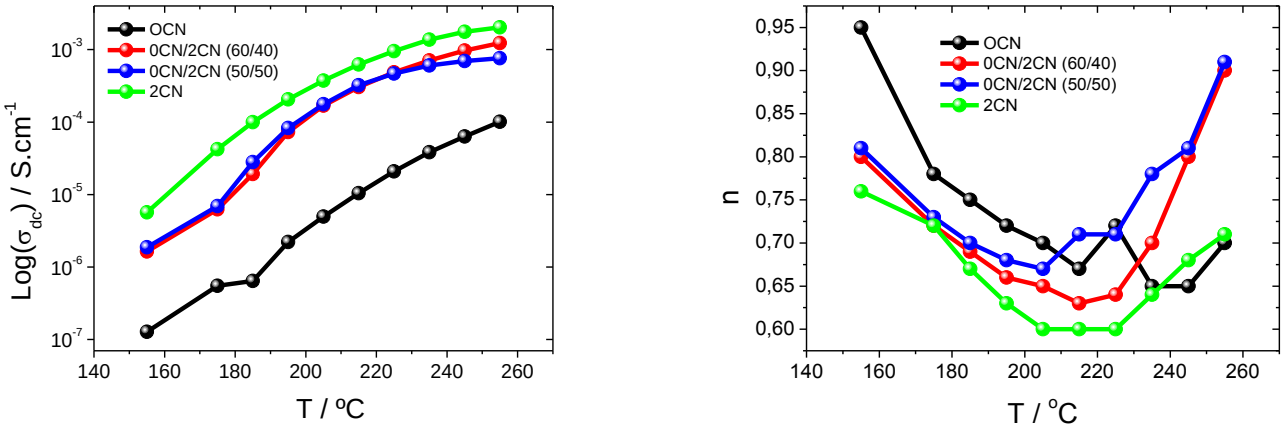

Figure 8 – σ_{dc} (left) and *n* (right) as a function of temperature for the different samples.

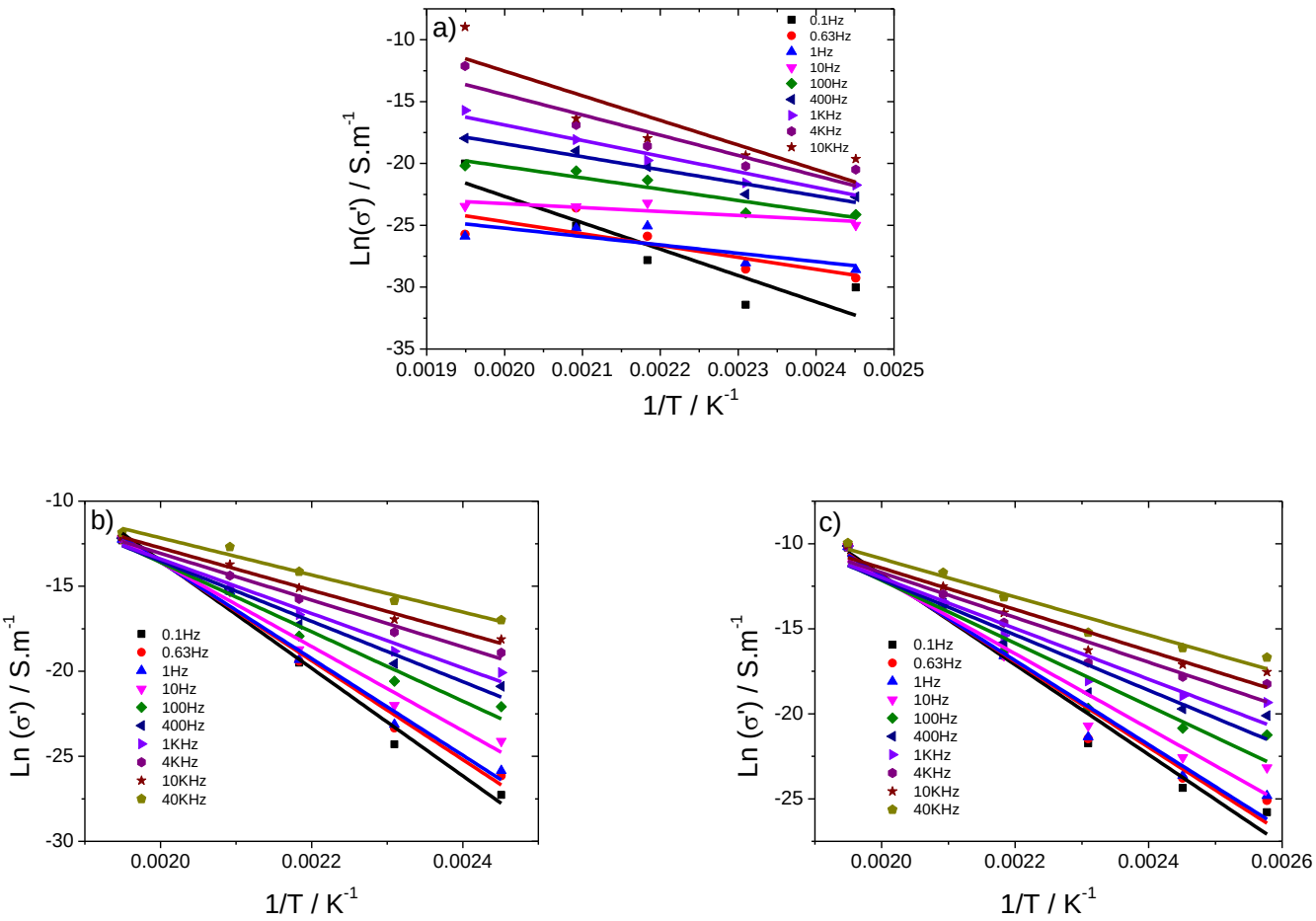

Figure 9 – Fitting of the electrical conductivity as a function of inverse temperature with the Dyre model: a) 0CN, b) 0CN/2CN (50/50) and c) 2CN.

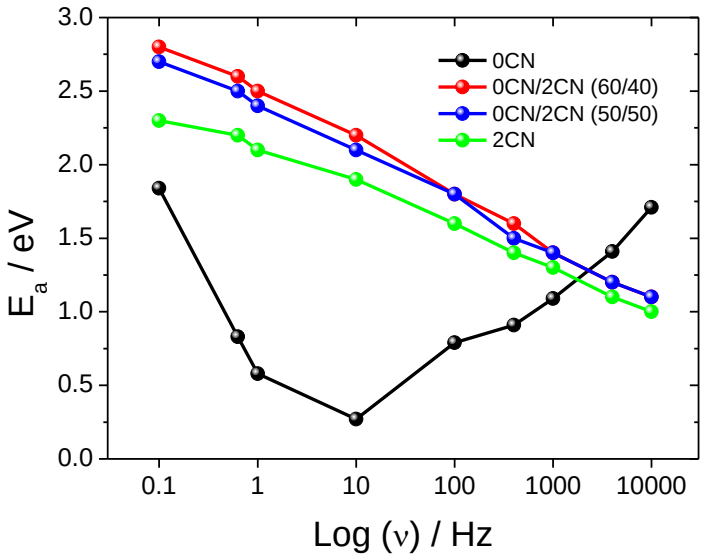

Figure 10 - Evolution of the activation energy as a function of frequency for the different samples.

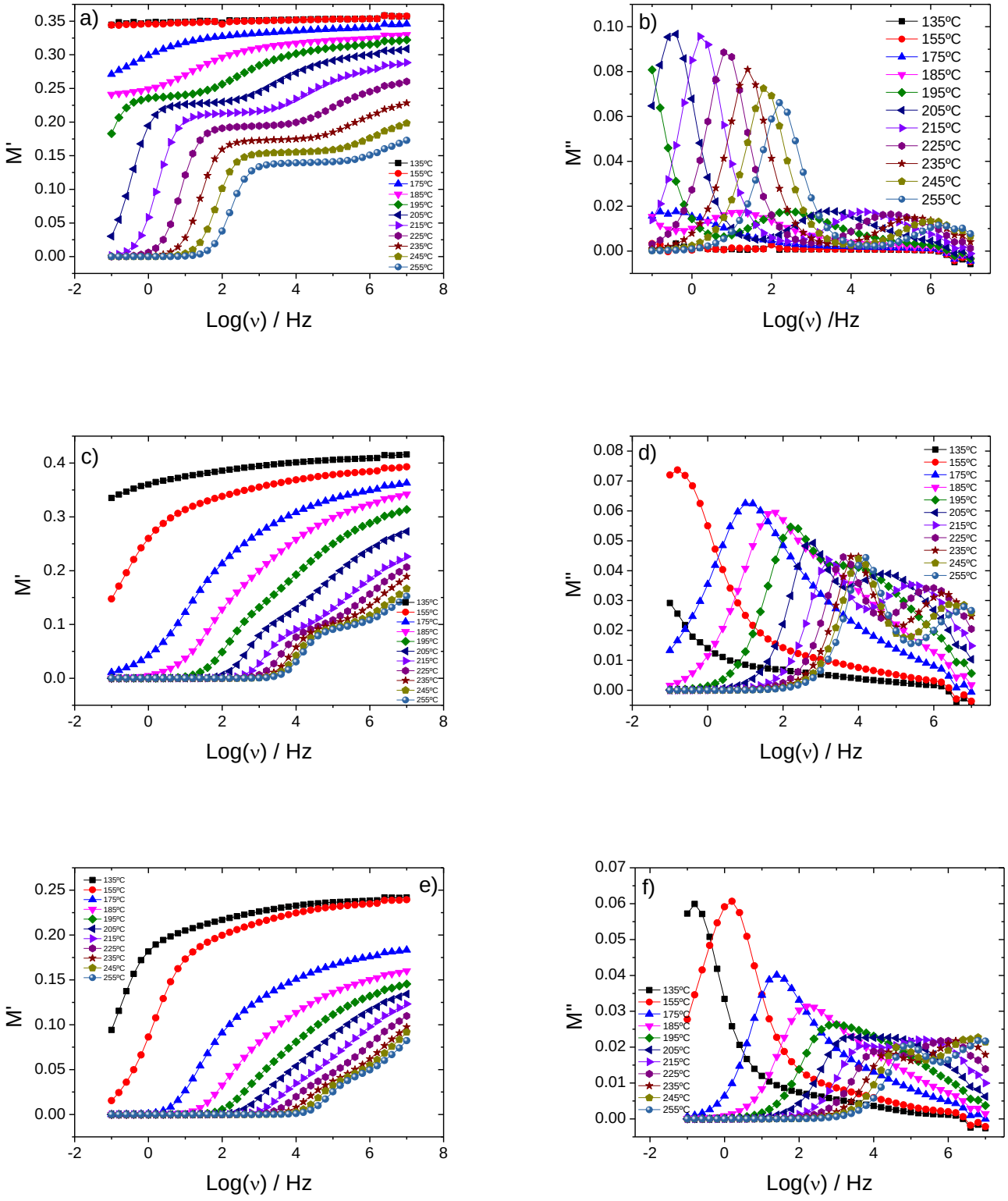

Figure 11 – Electric modulus (M´ and M´´) as function of frequency at different temperatures for: a-b) 0CN, c-d) 0CN/2CN (50/50), and e-f) 2CN.